Structure and Dynamics of Fluorescently Labeled Complex Fluids by Fourier Imaging Correlation Spectroscopy

by

Tyler Joshua Grassman

A THESIS

Presented to the Department of Chemistry
and the Honors College of the University of Oregon
in partial fulfillment of the requirements
for the degree of
Bachelor of Arts.

July 2000

Approved: 

Prof. Andrew H. Marcus

Abstract

An abstract of the Thesis of Tyler Joshua Grassman for the degree of Bachelor of Arts in the Department of Chemistry to be taken June 2000.

Title: STRUCTURE AND DYNAMICS OF FLUORESCENTLY LABELED COMPLEX FLUIDS BY FOURIER IMAGING CORRELATION SPECTROSCOPY

Presented here is a novel experimental method, Fourier imaging correlation spectroscopy (FICS), which performs phase-sensitive measurements of modulated optical signals from fluorescently labeled complex fluids. FICS experiments probe the time-dependent trajectory of a spatial Fourier component of the fluid particle density at a specified wavenumber k, and provide a direct route to the intermediate scattering function. The FICS approach overcomes signal sensitivity problems associated with dynamic light scattering, while offering a highly efficient means to acquire time-dependent information about spatial distributions of fluorescent particles, superior to direct imaging methods. Included is a description of the instrumental setup necessary to perform FICS experiments, the theory that establishes the connection between FICS observable and statistical mechanical quantities describing liquid state dynamics, and test measurements of monolayer suspension of fluorescent labeled polystyrene microspheres.

Table of Contents

Index of Figures

I. Introduction

Understanding the structure and dynamics of complex fluids and other so-called "soft materials" is of great fundamental importance and technological relevance. *Complex fluids* are fluids that are homogeneous at macroscopic scales and disordered at microscopic scales, but possess structure on a mesoscopic, or intermediate, length scale. Typical examples of complex fluids include surfactant solutions (such as micellar solutions and microemulsions), polymer solutions and melts, biological systems, and colloidal suspensions (such as ink, foam, and even milk). In colloidal suspensions, the mesoscopic length scale is the size of the colloid – a large, usually spherical, super-molecule made up of a long polymeric or extended solid substance – which is many times larger than the molecules that make up the suspending medium. Many of the unusual properties of complex fluids (liquid crystal phases, self-assembly, viscoelasticity, etc.) arise from the presence of a mesoscopic scale.

Of these unusual and important properties, the one of particular interest for our group is viscoelasticity, or more precisely, the molecular interactions that cause viscoelasticity. A viscoelastic material is, simply put, a substance that exhibits both viscous and elastic properties, and is best illustrated by use of a well-known example: silly putty. Silly putty has the amazing ability to be both bounced like a rubber ball and to be stretched and deformed like clay. This duality of properties is viscoelasticity. When rolled into a ball and tossed against a firm surface, the silly putty will bounce elastically, wherein the small deformations caused by the short-time stress of impact will be recovered, and the constituent molecules retain their original structure. However, if a long-time stress is applied to the silly putty, such as gradually squishing it or pulling it

apart, the molecules within will slowly slide by each other, just as in a viscous liquid, and any deformations created in the process will remain. These properties allow for viscoelastic materials to withstand a large amount of stress, and make them commercially and industrially very important, with an incredibly wide range of applications, such as airplane wings, kayaks, and biological implants.

Traditionally, experimental information about complex fluids and similar systems is obtained by a technique called *dynamic light scattering (DLS)*. In DLS, light shone into the sample material is scattered by periodic arrangements of atoms, molecules, or larger scattering centers, and the fluctuations of the scattered light intensity are monitored and recorded over time. From this information much can be discerned about the nature of microscopic and mesoscopic interactions within the complex fluid [Berne and Pecora, 1976; Pusey and Tough, 1985]. However, many important and interesting materials, such as biological systems, thin films, and membranes, have been left unstudied because of a lack of sufficient light scattering contrast (i.e. the scattering centers are too small or subtle, too much interference by other scattering centers than those of interest, etc.).

In order to overcome the failings of dynamic light scattering there have been a number of very useful and successful experimental techniques developed within the last few decades that have allowed for the study of complex systems to progress. Such techniques as digital video microscopy and fluorescence correlation spectroscopy have opened many doors that would have remained otherwise closed. Nevertheless, even these newer experimental methods have their drawbacks and/or limitations, as we shall see later in the sections following.

In response to these shortcomings, however, a new experimental technique for the study of complex fluids and other similar systems and materials has been independently developed by the Marcus group. This new approach, *Fourier imaging correlation spectroscopy (FICS)*, overcomes the sensitivity problems of DLS, as well as the deficiencies and disadvantages of other types of experiments, by isolating the fluctuations being measured in an *N*-body system to a single spatial frequency (or wavenumber, k). The basic FICS principle is illustrated for the simple case of a two-particle system in Figure 1. Figure 1A shows a schematic diagram of two uniformly labeled fluorescent particles (with diameter σ) exposed to an infinite periodic excitation grating that is directed along the x-axis. For the particle configuration shown, the x-component of the inter-particle separation, Δr_x, exactly matches the period of the grating, d_G. If the dark fringes correspond to the regions of the grating where the photon flux is greatest, the grating position shown on the left side of Figure 1A will result in the least possible number of chromophores being optically excited. The average fluorescence intensity emitted from the particles for this grating position will therefore be minimized. If the particles remain stationary while the position of the excitation grating is translated along the direction of the x-axis by the distance $d_G/2$ (a 180° phase shift), a maximal number of chromophores will be exposed to the excitation field and the resulting fluorescence intensity will be maximized. The variation of the fluorescence intensity of the system as a function of grating position is indicated schematically for two zero-to-2π cycles. The amplitude of the modulated fluorescence signal is maximized for this particle configuration ($\Delta r_x \approx d_G$) and its relative phase to that of the arbitrarily chosen position of the grating is zero.

We now consider the effect on the modulated fluorescence signal after the occurrence of a particle fluctuation. In Figure 1B is shown the same initial grating position as described above, however, the particle positions have changes so that Δr_x has decreased to a value slightly larger than $d_G/2$. For the particle configuration and grating position shown on the left side of Figure 1B, the fluorescence signal is maximized relative to other grating positions. As in the previous case, translation of the grating leads to modulation of the fluorescence signal. However, the amplitude of the modulation is now smaller than before since there is no grating position that can simultaneously excite all of the chromophores on the two particles. Thus, the particle fluctuation illustrated in Figure 1B results in a finite decrease in the modulation amplitude of the fluorescence signal and a finite increase in its relative phase with respect to the grating position.

Based on the above example, we can assign physical meanings to the FICS observables (phase and amplitude) and make a generalization to the same measurement performed on an *N*-body system. The amplitude of the modulated signal reflects the extent to which an *N*-body system contains spatial periodicity (or wave number, k) that matches the spatial frequency of the excitation grating ($k_G = 2\pi/d_G$). For the purpose of this work, we consider only isotropic fluid systems so that all orientations of the excitation grating (and hence, all directions of the wave vector, $\mathbf{k}_G$) yield equivalent information. The phase of the modulated signal reflects the relative position (or phase) of the spatial periodicity at wave number k_G contained by the particle configuration with respect to the reference position (or phase), of the excitation grating. It will be shown in later sections that measurements of the phase and amplitude performed as described above contain all of the information to fully characterize the spatial Fourier component of

the particle configuration at the spatial frequency k_G defined by the excitation grating. By performing many separate measurements corresponding to different values of $k = k_G$, the statistically relevant spatial and temporal distributions within the system can be readily determined.

In this paper I present the theory connecting the experimental observables of Fourier imaging correlation spectroscopy with the relevant statistical mechanical quantities of liquid-state dynamics and the experimental setup necessary to perform these experiments. Also presented are the results from a series of test measurements on Rhodamine-labeled 1μm polystyrene colloidal particles confined to monolayer suspensions, demonstrating the usefulness and accuracy of this new technique as a more direct and easily obtainable route to statistically relevant information than other popular experimental methods.

II. Background and Theory

1. Important Statistical Mechanical Quantities

The most convenient way to characterize the structure and dynamics of such complicated systems as complex fluids is to use statistical mechanics. Statistical mechanics is, as the name implies, a mathematical method of describing the microscopic actions and interactions of constituent "particles" and associating them with observed macroscopic properties in the bulk material. Statistical mechanical theory is one of the most important tools available to materials researchers, having the ability to describe a very wide range of interesting bulk properties, from magnetism and conductivity in metals, to the freezing and boiling of water.

There are a number of particularly informative statistical mechanical quantities used in the description of the structure and dynamics of complex fluids. The most basic of these is the *fluid particle number density*:

$$C(\mathbf{r},t) = \sum_{i=1}^{N} \delta[\mathbf{r} - \mathbf{r}_i(t)]. \qquad (1)$$

Thus, $C(\mathbf{r},t)$ contains information about the positions of the N particles contained in the system over the entire range of possible positions and through time. However, as the number of particles in the system increases, the amount of raw information contained here becomes quite vast and therefore very difficult to understand and process alone. Therefore, spatial and temporal ensemble averaged quantities are employed, which provide information in a more collective and understandable manner.

Probably the most important of the statistical quantities is the *intermediate scattering function*, defined as

$$F(k,\tau) = \left\langle \hat{C}^*(\mathbf{k},t)\hat{C}(\mathbf{k},t+\tau)\right\rangle \qquad (2)$$
$$= \sum_{ij}\left\langle \exp\left[i\mathbf{k}\cdot(\mathbf{r}_j(t+\tau)-\mathbf{r}_i(t))\right]\right\rangle - 8\pi^3\langle C\rangle\delta(\mathbf{k}).$$

The intermediate scattering function is the two-point time-correlation function of the Fourier components of the fluid particle number density, given by

$$\hat{C}(\mathbf{k},t) = \left(1/\sqrt{N}\right)\int d^3r\, e^{-i\mathbf{k}\cdot\mathbf{r}}C(\mathbf{r},t), \qquad (3)$$

where $\hat{C}(\mathbf{k},t) = \left|\hat{C}\right|\exp[i\alpha]$ is a complex number having both amplitude, $\left|\hat{C}\right|$, and phase, α.

The intermediate scattering function is an important quantity for a couple of reasons. The first of these is that it provides a good description of the k-space (inverse space) particle dynamics of the system, in the form of exponential decays, $e^{-D(k)k^2t}$, from which the k-dependant diffusion constant(s), D(k), may be extracted. For purely random diffusive motion, $F(k,\tau)$ will yield the free-particle diffusion constant, D_0. Thus, by analyzing $F(k,\tau)$ at different length- and time-scales one can monitor the affects of different system environments (i.e. temperature, density, geometry, etc.) on the motions of the constituent particles (i.e. diffusive motion, cage effects, etc.).

The other important quality of the intermediate scattering function is that it is the basis for the calculation of a number of other important statistical mechanical quantities (thus the "intermediate" designation). The zero-time limit of the intermediate scattering function contains information about the time averaged spatial distribution of particles, such as the average inter-particle spacing, and is known as the *static structure factor*:

$$S(k) = F(k,0) = 1 + \sum_{i,j\neq i}\left\langle \exp\left[-i\mathbf{k}\cdot\mathbf{r}_{ij}(t)\right]\right\rangle - 8\pi^3\langle C\rangle\delta(\mathbf{k}). \qquad (4)$$

Real-space dynamic and structural correlation functions can also be calculated from F(k,τ) and S(k). The *microscopic density-density time correlation function*, also known as the *van Hove correlation function*, can be reached via Fourier transformation of the intermediate scattering function:

$$G(r,\tau) = \int d^3k\, e^{ik\cdot r} F(k,\tau) = \sum_{ij} \left\langle \delta(\mathbf{r} + \mathbf{r}_i(t) - \mathbf{r}_j(t+\tau)) \right\rangle - \langle C \rangle \tag{5}$$

This function has the ability to probe either the dynamics of particles in terms of their displacement from their initial positions, or in terms of how the initial positions of particles effect the motions of neighboring particles. The *inter-particle pair correlation function*, g(r), can be also be reached via Fourier transformation, but of the static structure factor:

$$\langle C \rangle g(r) = \frac{1}{8\pi^3} \int d^3k\, e^{ik\cdot r} [S(k) - 1], = \sum_{i \neq j} \left\langle \delta(\mathbf{r} - \mathbf{r}_{ij}) \right\rangle \tag{6}$$

This function describes the statistical separations between a particle and it's nearest-neighbor shells, or "rings" of nearby particles.

When used in combination these statistical quantities provide for a thorough characterization of the microscopic structure and dynamics of even large, complicated systems. Since microscopic-scale interactions are the source of bulk properties, statistical mechanics is an all-important tool in the pursuit of understanding the true nature of the many interesting and exploitable attributes of both old and new materials.

2. Digital Video Fluorescence Microscopy (DVFM)

As mentioned before, the amount of information contained in the particle density function, C(**r**,t), given even a relatively small system over a similarly short time period, can become incredibly unwieldy. However, with the use of a computer, large amounts of information can be collected, stored, accessed, and analyzed with relative ease. It is therefore possible, in the case of certain systems, to study the actual constituent particles, and their motions, directly.

In order for such a study to be possible the particles of interest must actually be viewable, either by the naked eye or by way of a microscope. The introduction of fluorescent dyes, or chromophores, which are special molecules that emit light at a particular wavelength, or color, when light of another particular wavelength is shone upon them, provides for even better visualization. A camera connected to a computer can then record images, and even movies, of the particles within the system of study. These movies can then be analyzed using specialized computer algorithms to extract information about the microscopic properties of the system, including both particle trajectories and the previously discussed statistical mechanical quantities of importance. This extremely useful technique is know as *digital video fluorescence microscopy (DVFM)*, and has been used for many years with great success.

Figure 2A displays a digitized fluorescence image of a dense colloid suspension with areal density $\rho^* = N\sigma^2/A = 0.52$ ($N \approx 4160$ particles, contained in an area $A \approx 7850\mu m^2$). The x- and y-axes are orthogonal real-space coordinates. The picture is a physical representation of the instantaneous spatial particle density, C(r,0). Figure 2B shows a trajectory consisting of 20 consecutive particle configurations with an inter-

frame time step of 33msec. The trajectory data indicates that structural relaxation of local particle environments occur on this timescale, and that over a range of timescales (0.33msec < τ < 16sec), particles appear to be segregated into two populations; those oscillating within pseudo-hexagonally ordered local domains, and those "hopping" among adjacent sites within string-like channels [Marcus 1999]. This picture is a physical representation of the spatial particle density, C(r,t), over a small temporal range, t.

The spatial information contained in a single digitized image is equivalent to that contained by the Fourier transformation of the spatial particle density, $\hat{C}(\mathbf{k},t)$, as given by Eq. (3). Figure 2C displays the Fourier transform of the image shown in Figure 2A multiplied by its complex conjugate, where the x- and y-axes are orthogonal reciprocal-space coordinates (k_x and k_y) and the origin is placed at the center of the frame. This operation, averaged over all possible particle configurations, defines the static structure factor, S(k), as given by Eq. (4). The structure exhibited by S(k) is indicative of the important spatial frequencies that make up the image shown in Figure 2A.

In much the same manner, other important statistical quantities can be calculated from DVFM measurements. In Figure 3 is shown the intermediate scattering function, F(k,τ), calculated from Fourier decomposition of the particle trajectory according to Eq. (2), for the two-dimensional fluid previously described in Figures 2A, 2B, and 2C. Relaxations at the wavenumber k_{max}, corresponding to the first peak in S(k), have a complicated multi-exponential form. Observations of the particle trajectory indicate that this results from a superposition of spatially segregated processes. On the time scale of

this measurement (~ 3sec), there remains a residual correlation of structure at k_{max}, while no such structure persists at higher wavenumbers.

In Figures 4A and 4B is presented the self and distinct parts of the van Hove function, given by Eq. (5), calculated from the same DVFM as described in Figures 2 and 3. Note that $G_s(r,\tau)$ is a single-mode Gaussian distribution for the shortest τ sampled (33msec). For $0.033\text{sec} < \tau < 16\text{sec}$ the hopping processes observed in the particle trajectory lead to a non-Gaussian tail to develop in $G_s(r,\tau)$ at large distances, until the distribution regains a Gaussian form for $\tau > 16\text{sec}$. On this long timescale, the fluid appears dynamically homogeneous. The distinct part of the van Hove function reflects the relaxation of the structural information contained in the pair correlation function, g(r). The decay of $G_d(r,\tau)$ at the value of r corresponding to its first peak appears single-exponential until $\tau \sim 2\text{sec}$, at which time the nearest-neighbor structural relaxation is retarded. Structural changes at the second (and higher order) peaks, however, are arrested on much shorter timescales ($0 < \tau < 132\text{msec}$).

So, information collected via digital video fluorescence microscopy does in fact contain all the necessary information to completely characterize the dynamics of a complex fluid system. However, successful as this technique may be, it does have its drawbacks. First of all, the systems that can be easily studied without having to resort to the use of expensive supercomputers are quite small, on the order of only a few thousand particles (consider the fact that a single drop of water contains over 10^{21} molecules). However, even though the systems are small, the amount of digital information that must be stored can be immense. Also, with these larger systems (small as they actually may be), calculations of statistical quantities can often take a long time to complete, even on a

powerful computer. With these few, but significant, disadvantages to DVFM, it is important to search for new and more useable methods of study. But, even with the disadvantages, DVFM continues to be a very valuable tool, especially when used in conjunction with other experimental techniques, as shall be seen later on in this report.

3. Fourier Imaging Correlation Spectroscopy (FICS)

Conventional *fluorescence correlation spectroscopy (FCS)*, a highly useful experimental technique for the study of dynamics in complex fluids, has been around for nearly 30 years. While dynamic light scattering experiments require the fluids to possess relatively large scattering centers – this is the main reason DLS is an unusable technique with many systems – FCS requires only that some or all of the particles be either themselves fluorescent or be fluorescently dyed, which is often a relatively trivial task. Typically, in FCS measurements, a small spot within the chromophore-doped sample is illuminated and the resulting fluorescence intensity is monitored and recorded over time. As the chromophore density within this spot fluctuates, so does the resultant fluorescence intensity. This signal may then be time-correlated to give a final output proportional to the intermediate scattering function.

In order to improve upon the sensitivity and selectivity of the information being probed by these experiments, we have developed a related, yet greatly superior technique, which we call *Fourier imaging correlation spectroscopy (FICS)*. In FICS experiments, like in conventional FCS experiments, the motion of the chromophore-labeled particles is detected as slow fluctuations in fluorescence intensity. However, in FICS experiments the sample is probed with an oscillatory excitation pattern (an optically generated grating)

which stretches over a many times larger sample region than the small laser spot of conventional FCS experiments. The excitation pattern is created by the phase-interference of two linearly polarized laser beams brought to a focus at the sample plane of a fluorescence microscope. The period of the fringe pattern (i.e. the distance between two consecutive bright or dark regions), d_G, depends on the intersection angle, φ, between the two beams [Fleming, 1986], and can be varied continuously from tens of microns ($1\mu m = 10^{-6}m$) to $\lambda_{ex}/2$:

$$d_G = \frac{\lambda_{ex}}{2\varsigma \sin(\varphi/2)}, \tag{7}$$

where ς is a correction factor accounting for different indices of refraction resulting from the laser beams passing through multiple optical surfaces (see the following experimental section). The size of the illuminated region is determined by the waist of the crossed laser beams at their focus, $w \approx 100\mu m$.

In similar fashion to Taylor or Laurent series, a Fourier series is an expansion of a function into a sum of individual Fourier component functions. This mathematical property helps make up the theoretical basis of what sort of information FICS experiments are able to probe in a sample system. At any instant in time, the oscillatory excitation profile picks out a small set of spatial Fourier components of the fluorescent-labeled particle distribution. There is a primary component at wavenumber (a measure of inverse space) $k_G = |\mathbf{k}_G| = 2\pi d_G^{-1}$, in addition to a $|\mathbf{k}| = 0$ component associated with the mean fluorescent light level, and a band of small-k contributions associated with the actual size of the illuminated region. Temporal fluctuations in the fluorescence intensity reflect the growth and decay of the spatial Fourier components of the illuminated region.

Slow fluctuations in the chromophore distribution corresponding to small-k spatial components arise from particles moving in and out of the sample region of interest. Other components of the signal include those resulting from slow drifts in laser alignment, low frequency mechanical vibrations, and detector electronic noise.

Fluctuations of the signal due solely to fluctuations in the number density, $C(\mathbf{r},t)$, at wavenumber k_G are selectively measure using the lock-in detection method [Harrowitz and Hill, 1986]. A frequency generator is used to modulate the phase of the excitation fringe pattern from 0 to 2π at the angular frequency ω_G. The pattern is thus swept across the illuminated sample region at a velocity, $\upsilon_G = \omega_G/k_G$, greater than that at which a particle can travel the distance equal to the period of the fringe, $d_G = 2\pi k_G^{-1}$. The resulting integrated fluorescence intensity that emerges from the sample region is also modulated at the frequency ω_G. Because the continuous and periodic sweeping of the fringe pattern over the distance d_G induces the signal modulation, this part of the signal is sensitive to density fluctuations on the same length scale. The lock-in detection method (explained below) determines the signal modulation at precisely the frequency ω_G, and ignores all signal contributions at other frequencies ($\omega \neq \omega_G$). Thus, all components to the signal that are not correlated with the modulation frequency (including noise and density fluctuations corresponding to $k \neq k_G$) are excluded from the measurement.

The physical meaning of the modulated signal can be understood if we consider the total instantaneous fluorescence intensity, $I_G(t)$. This quantity arises from the spatial overlap of the oscillatory excitation profile (the optical grating), $I_{ex}(\mathbf{r})$, and the time-dependent density of fluorescently labeled particles, $C(\mathbf{r},t)$:

$$I_G(t) = \varkappa \int C(\mathbf{r},t) I_{ex}(\mathbf{r}) d^3r = \varkappa \int \hat{C}(\mathbf{k},t) \hat{I}_{ex}(\mathbf{k}) d^3k. \qquad (8)$$

$\hat{C}(\mathbf{k},t)$ is the Fourier transform of C(r,t), given by Eqs. (1) and (3), and κ is a proportionality factor accounting for the absorption cross section, quantum yield, and light collection efficiency of the experimental system.

Since the laser beam waist is significantly larger than d_G, the excitation profile can be approximated as an infinite two-dimensional fringe pattern in the direction of the x-axis:

$$\begin{aligned} I_{ex}(\mathbf{x}) &= I_0\{1+\cos[\mathbf{k}_G\cdot\mathbf{x}+\phi(t)]\} \\ &= I_0\left\{1+\tfrac{1}{2}\left[e^{i(k_G\cdot x+\phi)}+e^{-i(k_G\cdot x+\phi)}\right]\right\}, \end{aligned} \tag{9}$$

where the Euler formula, $\cos\psi = \frac{1}{2}\left[e^{i\psi}+e^{-i\psi}\right]$, has been used and I_0 is the constant total laser intensity level. The interference fringe pattern, then, can be described as a cosine "waveform" whose amplitude ranges from 0 to $2I_0$. The time-dependent phase of this grating, $\phi(t) = \omega_G t + \theta_G = \mathbf{k}_G\cdot\upsilon_G t + \theta_G$, completes a 0 to 2π cycle (which causes the sweeping motion of the interference fringe pattern) at the angular frequency ω_G, where the direction of $\mathbf{k}_G$ is opposite to that of υ_G, and θ_G is a constant.

The Fourier transformation of the excitation profile, $I_{ex}(\mathbf{x})$, then goes as:

$$\begin{aligned} \hat{I}_{ex}(\mathbf{k}) &= \tfrac{1}{2\pi}\int e^{ik\cdot x} I_{ex}(\mathbf{x})dx \\ &= \tfrac{I_0}{2\pi}\left[\int e^{ik\cdot x}dx + \tfrac{1}{2}\int e^{ik\cdot x}e^{i(k_G\cdot x+\phi)}dx + \tfrac{1}{2}\int e^{ik\cdot x}e^{-i(k_G\cdot x+\phi)}dx\right] \\ &= \tfrac{I_0}{2\pi}\left[\int e^{ik\cdot x}dx + \tfrac{1}{2}e^{i\phi}\int e^{i(k+k_G)\cdot x}dx + \tfrac{1}{2}e^{-i\phi}\int e^{i(k-k_G)\cdot x}dx\right] \\ &= I_0\left[\delta(\mathbf{k}) + \tfrac{1}{2}e^{i\phi}\delta(\mathbf{k}+\mathbf{k}_G) + \tfrac{1}{2}e^{-i\phi}\delta(\mathbf{k}-\mathbf{k}_G)\right], \end{aligned} \tag{10}$$

where the definition of a Dirac delta function, $\delta(\mathbf{v}) = \frac{1}{2\pi}\int e^{iu\cdot v}du$, is used. Thus, by the previous equation, we can see that the excitation profile is composed of a stationary zero-k contribution (the mean excitation light level), and modulated components corresponding to $\mathbf{k} = \pm\mathbf{k}_G$.

Next, Eq. (10) is substituted into Eq. (8), giving:

$$\begin{aligned} I_G(t) &= \varkappa I_0\Big[\int \hat{C}(\mathbf{k},t)\delta(\mathbf{k})dk + \tfrac{1}{2}e^{i\phi}\int \hat{C}(\mathbf{k},t)\delta(\mathbf{k}+\mathbf{k}_G)dk \\ &\quad + \tfrac{1}{2}e^{-i\phi}\int \hat{C}(\mathbf{k},t)\delta(\mathbf{k}-\mathbf{k}_G)dk\Big] \\ &= \varkappa I_0\Big[\hat{C}(0) + \tfrac{1}{2}e^{i\phi}\hat{C}(\mathbf{k}_G,t) + \tfrac{1}{2}e^{-i\phi}\hat{C}^*(\mathbf{k}_G,t)\Big]. \end{aligned} \tag{11}$$

The fact that $\hat{C}(\mathbf{k},t)$ is a complex number is used here in order to write $\hat{C}(-\mathbf{k},t)$ as $\hat{C}^*(\mathbf{k},t)$, by definition of the complex conjugate. This allows us to further simplify $I_G(t)$:

$$\begin{aligned} I_G(t) &= \varkappa I_0\Big\{\hat{C}(0) + \tfrac{1}{2}\Big[e^{i\phi}\big|\hat{C}\big|e^{i\alpha} + e^{-i\phi}\big|\hat{C}\big|e^{-i\alpha}\Big]\Big\} \\ &= \varkappa I_0\Big\{\hat{C}(0) + \tfrac{1}{2}\big|\hat{C}\big|\Big[e^{i(\phi+\alpha)} + e^{-i(\phi+\alpha)}\Big]\Big\} \\ &= \varkappa I_0\Big\{\hat{C}(0) + \big|\hat{C}\big|\cos[\phi+\alpha]\Big\} \\ &= \varkappa I_0\Big\{\hat{C}(0) + \big|\hat{C}(\mathbf{k}_G,t)\big|\cos[\omega_G t + \theta_G + \alpha(\mathbf{k}_G,t)]\Big\}, \end{aligned} \tag{12}$$

where α is the phase angle associated with $\hat{C}(\mathbf{k},t)$, given by $\alpha = \tan^{-1}\left[\mathrm{Im}\,\hat{C}/\mathrm{Re}\,\hat{C}\right]$. Figure 5A shows a schematic illustration of the modulated signal, along with the reference oscillatory waveform used to generate the modulation, $\sin[\phi_{ref}(t)]$, where $\phi_{ref}(t) = \omega_{ref}t + \theta_{ref}$ and $\omega_{ref} = \omega_G$. The phase shift between the signal and reference waveforms is $\theta_{ref} - \theta_G + \alpha$. Equation (12) shows that the total signal is composed of a stationary and a modulated component. The stationary component, $\varkappa I_0\hat{C}(0)$, corresponds to the mean fluorescence background, while the modulated component contains information about $\hat{C}(\mathbf{k}_G,t)$ via its modulus, $\big|\hat{C}\big|$, and phase angle, α (please see Appendix A for a discussion on the physical meaning of the modulus and phase angle).

Because fluctuations of $\hat{C}(\mathbf{k}_G,t)$ occur at lower frequencies than that of the reference modulation, the lock-in amplifier can be used to demodulate the signal into slowly varying complex components, X(t) and Y(t), defined by the phase sensitive

detection method [Horowitz and Hill, 1986]. This is accomplished by multiplying the signal [Eq. (12)] by the reference waveform, phase-shifted by 0° [$\sin(\phi_{ref})$] and 90° [$\cos(\phi_{ref})$], respectively, and then employing a low-pass filter. This is equivalent to performing the following mathematical operations:

$$X(t) = \frac{1}{\tau_{LI}} \int_{-\infty}^{t} ds\, I_G(s) \sin[\phi_{ref}(s)] e^{-(t-s)/\tau_{LI}} \tag{13}$$

$$Y(t) = \frac{1}{\tau_{LI}} \int_{-\infty}^{t} ds\, I_G(s) \cos[\phi_{ref}(s)] e^{-(t-s)/\tau_{LI}},$$

where the lock-in time constant, τ_{LI}, and θ_{ref} are experimentally adjustable parameters, and s is the dummy variable of integration. Upon substitution of Eq. (12) into Eq. (13), we find that the modulated parts of the integrands have the forms

$$\left|\hat{C}\right| \cos[\omega_G s + \theta_G + \alpha] \sin[\omega_{ref} s + \theta_{ref}] \quad \text{for X(t), and} \tag{14}$$

$$\left|\hat{C}\right| \cos[\omega_G s + \theta_G + \alpha] \cos[\omega_{ref} s + \theta_{ref}] \quad \text{for Y(t).}$$

Using the trigonometric identities $\cos(x)\sin(y) = \frac{1}{2}[\sin(x+y) - \sin(x-y)]$ and $\cos(x)\cos(y) = \frac{1}{2}[\cos(x+y) - \cos(x-y)]$, we find that these integrands contain both oscillatory sum- and difference-frequency terms:

$$\tfrac{1}{2}\left|\hat{C}\right| \{\sin[(\omega_G + \omega_{ref})s + \theta_G + \theta_{ref} + \alpha] - \sin[(\omega_G - \omega_{ref})s + \theta_G - \theta_{ref} + \alpha]\}, \text{ and} \tag{15}$$

$$\tfrac{1}{2}\left|\hat{C}\right| \{\cos[(\omega_G + \omega_{ref})s + \theta_G + \theta_{ref} + \alpha] - \cos[(\omega_G - \omega_{ref})s + \theta_G - \theta_{ref} + \alpha]\}$$

for X(t) and Y(t), respectively. When τ_{LI} is set to a value much smaller than the timescale of the fluctuations of $\hat{C}(\mathbf{k}_G, t)$, the integration described by Eq. (13) has the effect of removing all the AC components of the signal, while the DC components remain. In other words, we filter out the portions of the total signal that are not concerned with our signal of interest, the fluctuations of $\hat{C}(\mathbf{k}_G, t)$. Since our reference

and signal waveforms have the same frequencies ($\omega_G = \omega_{ref}$), the sum-frequency terms in Eq. (15) are removed by the low-pass filter, and the difference-frequency terms survive. Thus, evaluation of Eq. (13) leads to

$$\begin{aligned} X(t) &= \tfrac{\varkappa I_0}{2\tau_{LI}}\left|\hat{C}\right|\sin(\theta-\alpha) = \tfrac{\varkappa I_0}{2\tau_{LI}}\left|\hat{C}\right|\left(\cos\alpha\sin\theta - \sin\alpha\cos\theta\right) \\ &= \tfrac{\varkappa I_0}{2\tau_{LI}}\left\{\mathrm{Re}\left[\hat{C}\right]\sin\theta - \mathrm{Im}\left[\hat{C}\right]\cos\theta\right\} \\ Y(t) &= \tfrac{\varkappa I_0}{2\tau_{LI}}\left|\hat{C}\right|\cos(\theta-\alpha) = \tfrac{\varkappa I_0}{2\tau_{LI}}\left|\hat{C}\right|\left(\cos\alpha\cos\theta - \sin\alpha\sin\theta\right) \\ &= \tfrac{\varkappa I_0}{2\tau_{LI}}\left\{\mathrm{Re}\left[\hat{C}\right]\cos\theta - \mathrm{Im}\left[\hat{C}\right]\sin\theta\right\}, \end{aligned} \tag{16}$$

where $\theta = \theta_{ref} - \theta_G$ is the constant, though relatively short, time lag associated with the detection of fluorescence after it has been emitted from the sample. θ, then, can be set to any arbitrary value by adjusting θ_{ref}.

Equation (16) shows that X and Y are each a function of the particle coordinates through their relationship to $\hat{C}(\mathbf{k}_G, t)$, and may therefore be considered dynamical variables of the N particle system [Hansen and McDonald, 1991]. The real and imaginary parts of $\hat{C}(\mathbf{k}_G, t)$ can be isolated separately in X and Y if θ is chosen to be an integer multiple of 90° or zero. Since the excited state lifetime of the Rhodamine chromophores used in these studies are $\sim 10^{-9}$sec and the electronic delays in the equipment are short, $\theta_G \approx 0$. Thus, the phase shift can be arbitrarily adjusted such that $\theta = 90°$. Under these circumstances, $\cos\theta = 0$ and $\sin\theta = 1$, and thus $X(t) = \varkappa I_0 \mathrm{Re}\left[\hat{C}\right]/2\tau_{LI}$ and $Y(t) = \varkappa I_0 \mathrm{Im}\left[\hat{C}\right]/2\tau_{LI}$. Figure 5B shows a schematic representation of the complex components of the demodulated signal for this case. Fluctuations of the vector $\mathbf{R}(t) = X(t) + iY(t)$ in the complex plane thus arise as a consequence of the fluctuations of

$\hat{C}(\mathbf{k}_G, t)$. The trajectory of **R** can then be used to calculated all of the time-correlation functions associated with $\hat{C}(\mathbf{k}_G, t)$.

The temporal and spatial two-point correlation functions of the complex fluid, $F(k,\tau)$ and $G(r,\tau)$, can be determined from measurements of X(t) and Y(t) without explicit knowledge of the phase angles, θ and α. Using the definition of $F(k,\tau)$ from Eq. (2) and $\hat{C}(\mathbf{k}_G, t) = \mathrm{Re}[\hat{C}] + i\,\mathrm{Im}[\hat{C}]$,

$$\begin{aligned} F(k,\tau) &= \left\langle \hat{C}(k,t)\hat{C}^*(k,t+\tau) \right\rangle \\ &= \left\langle \left\{ \mathrm{Re}[\hat{C}(k,t)] + i\,\mathrm{Im}[\hat{C}(k,t)] \right\} \left\{ \mathrm{Re}[\hat{C}(k,t+\tau)] - i\,\mathrm{Im}[\hat{C}(k,t+\tau)] \right\} \right\rangle \\ &= \left\langle \mathrm{Re}[\hat{C}(k,t)]\mathrm{Re}[\hat{C}(k,t+\tau)] + \mathrm{Im}[\hat{C}(k,t)]\mathrm{Im}[\hat{C}(k,t+\tau)] \right. \\ &\qquad \left. + i\,\mathrm{Im}[\hat{C}(k,t)]\mathrm{Re}[\hat{C}(k,t+\tau)] - i\,\mathrm{Im}[\hat{C}(k,t+\tau)]\mathrm{Re}[\hat{C}(k,t)] \right\rangle \\ &= \left\langle \mathrm{Re}[\hat{C}(k,t)]\mathrm{Re}[\hat{C}(k,t+\tau)] \right\rangle + \left\langle \mathrm{Im}[\hat{C}(k,t)]\mathrm{Im}[\hat{C}(k,t+\tau)] \right\rangle . \end{aligned} \tag{17}$$

To reach the final form of this equation we have used the fact that the function $\hat{C}(\mathbf{k}_G, t)$ has a special property of symmetry, which causes the cross-terms to cancel out.

The time-correlation function of the dynamical variable X(t), then, has the form

$$\begin{aligned} \langle X(t)X(t+\tau) \rangle &= \tfrac{x^2 I_0^2}{4\tau_{LI}^2} \left\langle \left\{ \mathrm{Re}[\hat{C}(k,t)]\sin\theta - \mathrm{Im}[\hat{C}(k,t)]\cos\theta \right\} \right. \\ &\qquad \left. \times \left\{ \mathrm{Re}[\hat{C}(k,t+\tau)]\sin\theta - \mathrm{Im}[\hat{C}(k,t+\tau)]\cos\theta \right\} \right\rangle \\ &= \tfrac{x^2 I_0^2}{4\tau_{LI}^2} \left\langle \mathrm{Re}[\hat{C}(k,t)]\mathrm{Re}[\hat{C}(k,t+\tau)]\sin^2\theta \right. \\ &\qquad \left. + \mathrm{Im}[\hat{C}(k,t)]\mathrm{Im}[\hat{C}(k,t+\tau)]\cos^2\theta \right\rangle , \end{aligned} \tag{18}$$

where the cross-terms cancel for the same reason as given for Eq. (17). A similar expression describes the time-correlation function for the variable Y(t):

$$\begin{aligned} \langle Y(t)Y(t+\tau) \rangle = \tfrac{x^2 I_0^2}{4\tau_{LI}^2} \left\langle \right. & \mathrm{Re}[\hat{C}(k,t)]\mathrm{Re}[\hat{C}(k,t+\tau)]\cos^2\theta \\ & \left. + \mathrm{Im}[\hat{C}(k,t)]\mathrm{Im}[\hat{C}(k,t+\tau)]\sin^2\theta \right\rangle . \end{aligned} \tag{19}$$

Comparison of Eqs. (17), (18), and (19) reveals that

$$F(k,t) = \left\langle \mathrm{Re}\left[\hat{C}(k,t)\right]\mathrm{Re}\left[\hat{C}(k,t+\tau)\right]\right\rangle + \left\langle \mathrm{Im}\left[\hat{C}(k,t)\right]\mathrm{Im}\left[\hat{C}(k,t+\tau)\right]\right\rangle \qquad (20)$$
$$= \frac{\kappa^2 I_0^2}{4\tau_{LI}^2}\left\{\left\langle X(t)X(t+\tau)\right\rangle + \left\langle Y(t)Y(t+\tau)\right\rangle\right\}$$

Thus, analysis of the trajectories of the dynamical variables X and Y via Eq. (20) provide a direct route to the intermediate scattering function, which is a fundamental quantity of interest to the theoretical description of liquid state dynamics. And, of course, the static structure function is simply the zero-time ($\tau = 0$) limit of Eq. (20):

$$S(k) = \left\langle \hat{C}(k)\hat{C}^*(k)\right\rangle = \left\langle \mathrm{Re}^2\left[\hat{C}\right]\right\rangle + \left\langle \mathrm{Im}^2\left[\hat{C}\right]\right\rangle = \frac{\kappa^2 I_0^2}{4\tau_{LI}^2}\left\{\left\langle X^2\right\rangle + \left\langle Y^2\right\rangle\right\} \qquad (21)$$

III. Experimental Setup

The primary sample system of concern in this paper consists of 1μm diameter carboxylic acid functionalized polystyrene microspheres doped with red (580/605nm) fluorescent dye (Fluospheres, Molecular Probes). The microspheres, which come in an aqueous suspension containing 2% solids, are washed free of any surfactant impurities by dialysis in nanopure water for two days. They are then gently sedimented via microcentrifugation and resuspended in 20μM aqueous sodium decyl sulfate (an small ionic surfactant to stabilize the negatively charged particles against aggregation) and 100μM aqueous sodium azide (for ionic stabilization, and as an antibiotic to prevent microorganism growth inside the sample) at whatever particle density desired.

Because we desire to study confined liquid systems at particular sample thicknesses, a special adjustable micron-gap capillary sample cell is employed, seen pictorially in Figure 6. This piece consists, essentially, of two smooth, parallel glass surfaces (a 0.125" glass window on top and a No.1 glass microscope coverslip on the bottom), with hydrophobic octadecylsilane coatings (Glassclad-18, United Chemical Technologies) to prevent the hydrophilic microspheres from adhering to the naturally hydrophilic glass surfaces. The glass surfaces are held at a fixed distance apart by spring-loaded stainless steel plates, and can be slowly drawn together through the use of three independently controlled motorized micrometers (Picomotor, New Focus). This setup allows for adjustments of the sample thickness at increments of approximately 0.1μm. A small amount of the sample suspension (~50μL) is placed into the sample reservoir, whose bottom is the glass coverslip. The outside edge of the cell is then wrapped in a thin sheet of latex in order to create a water-tight barrier against solvent evaporation,

giving the average sample a lifetime of about five days. The crossing laser beams enter the sample cell through an aperture in the top plate and the fluorescence signal is collected by a microscope objective positioned beneath the bottom plate.

The laser system used by both the DVFM and FICS experiments is detailed graphically in Figure 7. The base of the system is a mode-locked Nd:YAG laser (Model 3100, Spectra Physics) that is frequency-doubled to produce green 532nm laser light. The beam is then split into two equal strength beams by way of Fresnel-rhomb prism and a polarizing beam splitter, which are repolarized using a periscope to obtain two *p*-polarized beams. One of these beams is passed through an electro-optic phase-modulator (Conoptics) being driven by a digital function generator (Keithley), where its phase is modulated from 0 to 2π at a rate of 50kHz (50,000Hz). The two beams are then focused onto the sample plane with 50cm focal length lenses, where the resulting fluorescence is then collected with a 100X fluorescence oil-immersion microscope objective (Leica, Plan Fluotar, Na = 1.3) and 5X eyepiece (Zeiss).

From the eyepiece the fluorescence can either be directed one of two places, depending upon the experiment to be performed. For the DVFM experiments the fluorescence is directed straight into a CCD camera (Cohu). The signal from the CCD is sent to a UNIX workstation (Indy R5000, Silicon Graphics) equipped with standard video capture hardware and software. This data is collected in the form of a movie at a frame rate of 10Hz. Using the workstation software, the movie is split into a series of images, which are then digitally filtered and further analyzed using IDL (Research Systems, Inc.), a programming language optimized for visual data analysis. The pixel length is calibrated by imaging a transmission electron microscope (TEM) grid of known scale.

The pixel dimension was calculated as 1 pixel = 0.1111 ± 0.0015μm. This calibration was checked by comparison of DVFM measurements of various fringe spacings with the corresponding values obtained using Eq. (7), which were found to have excellent agreement (see Figure 8, in which the theoretical calibration is given by the solid line and the DVFM measurements given by the solid circles).

For the FICS experiments the sample fluorescence is coupled into multi-mode optical fiber (3M) and transmitted onto a thermoelectrically cooled high-sensitivity photomultiplier tube (Hamamatsu, R3896) after filtration by a 590nm central wavelength band-pass filter (CVI Laser Optics, 10nm bandwidth, 90% transmission efficiency) and a 532nm notch filter (CVI Laser Optics). The signal from the PMT is demodulated with a dual-phase digital lock-in amplifier (SR830, Stanford Research Systems) that is referenced to the signal waveform used to drive the phase modulator. The resulting analog signals (total fluorescence, X, and Y) are then sent to a PC equipped with a high bandwidth analog-to-digital conversion/data acquisition card (MIO-16-1-E, National Instruments) and collected via National Instruments' Labview data acquisition/analysis software.

Typically, for each FICS experiment, 32,000 data points are collected at an acquisition frequency of 512Hz. Individual data sets are repeated 10-20 times, and after analysis, cross-checked for consistency, and averaged together. Analysis consists of individual time-correlation of the X and Y trajectories by averaging over t_{max} time origins according to

$$\langle A(t)A(t+\tau)\rangle = \frac{1}{t_{max}}\sum_{t_0=1}^{t_{max}} A(t_0)A(t_0+\tau), \tag{22}$$

where A = X, Y. The decay time of the autocorrelation function is a measure of the time required for a labeled particle to move the distance k_G^{-1}. The upper limit to the temporal resolution of FICS measurements is determined by the modulation frequency. Essentially, 10 cycles of the reference oscillator are necessary to determine a single data point. For the experiments presented here, a modulation frequency of 50kHz was used, corresponding to an instrument time resolution of 200μsec.

IV. Results and Discussion

In Figure 9A is shown a typical raw data set taken from FICS measurements performed on a dilute monolayer suspension of red-fluorescent-labeled colloidal spheres (diameter, $\sigma = 1\mu m$) with number density, $\rho^* = N\sigma^2/A = 0.02$ ($N \approx 160$ particles contained by an area $A \approx 7850\mu m^2$). At this low density, the mean inter-particle separation is large, [$L = (\rho^*/\sigma^2)^{-1/2} \approx 7.1\mu m$], such that the system behaves like a superposition of non-interacting Brownian particles for $d_G < L$. Or in other words, at length-scales smaller than the mean inter-particle separation the colloidal spheres act as though they are free particles being randomly pushed around by thermally induced solvent motions.

The signal trajectory shown in Figure 9A consists of 2,000 sequential points each separated by 2msec. For the purpose of clarity, line segments connecting adjacent time-points have been omitted. The signal has a symmetric distribution in the complex plane. The phase angle, α, spans the entire range between 0 and 2π, while the static distribution fits well to symmetric Gaussian functions of the X- and Y-coordinates. Table 1 summarizes the best-fit variances corresponding to similar data sets performed at successively increasing fringe spacing. The distribution width, which is proportional to S(k) according to Eq. (21), is insensitive to the fringe spacing for $\sigma \leq d_G \leq L$.

In Figure 9B are shown calculations [according to Eq. (20)] of the normalized intermediate scattering function corresponding to the trajectory data sets listed in Table 1. Under these dilute conditions, the particles are considered to be non-interacting, and the intermediate scattering function takes the Gaussian form [Berne and Pecora, 1976]:

$$F_s(k,\tau) = \exp[-k^2 D_s \tau], \qquad (23)$$

where $F_s(k,\tau)$ is the self-part of the intermediate scattering function and D_s is the self-diffusion coefficient. The data shown in Figure 9B decays in time as a single exponential and scales with wavenumber as a Gaussian, in precise agreement with the theoretical prediction. The solid lines correspond to Eq. (23) with $D_s = 3 \times 10^{-9}$ cm^2sec^{-1}. This value for the self-diffusion coefficient is in good agreement with that of the free diffusion coefficient, $D_0 = 0.707k_BT/6\pi\eta a = 3.1 \times 10^{-9}$ cm^2sec^{-1}, calculated from the Stokes-Einstein equation (with the necessary correction to account for the hydrodynamic friction due to the effect of the cell walls).

When experiments are performed on a more dense system, the dynamics are complicated by multi-exponential decays that vary with k. In Figure 10A is shown plots of $F(k,\tau)/S(k)$ as a function of time for a denser monolayer colloidal suspension ($\rho^* = 0.31$). Similar to dynamic light scattering, FICS is capable of accurately characterizing non-exponential relaxations of the intermediate scattering function. This is an important advantage over alternate fluorescence detection methods where direct measurement of $F(k,\tau)/S(k)$ is not possible [Davoust, 1982]. Thus, we expect this approach to be a useful means to obtain experimental information about the scaling of power-law exponents as a function of time and wavenumber.

Using microscopic particle trajectories extracted from DVFM experiments, it is possible to calculate the normalized intermediate scattering function, $F(k,\tau)/S(k)$, for the range of k and τ being represented by the video images. In Figure 10A is shown the results of this calculation (represented by the empty circles) for the k values corresponding to FICS experiments (represented by the solid lines) performed on the same dense monolayer colloidal suspension ($\rho^* = 0.51$). This overlay shows a high

degree of correspondence amongst the values yielded by the two different experimental techniques.

It is also possible to perform the same sort of analysis for the static structure factor, S(k). An overlay of the normalized $S(k_G)$ values calculated from FICS data according to Eq. (21) for this same system (represented in Figure 10B by the filled circles) on the S(k) calculated from DVFM data (represented by the solid line) again shows very good agreement by the two experiments.

Because of its low excitation power requirements and high sensitivity, FICS is ideally suited for studying the dynamics of biological systems, such as intracellular motion. It has recently been applied to measure the translocation of organelles in live cells [Margineantu, 2000]. Figure 11 shows the results of FICS measurements performed on human osteosarcoma cells (a type of cancer) in which the mitochondria have been fluorescent- labeled. Mitochondria exist in these cells as a single semi-dilute network of entangled tube-like filaments (~ 0.5 μm diameter cross section), which are plastic-like and constantly undergo changes in shape. The plots of the "effective" diffusion coefficient are constructed from Eq. (11) with $\tilde{D}_{eff}(k,\tau) = D_s$. For the three wavenumbers examined, $\tilde{D}_{eff}(k,\tau)$ relaxes on the characteristic time scale $\tau_1 \sim 15$ sec and exhibits a sensitivity to k that results from a structural rearrangement of the local mitochondrial filament environment in the range of length scales $0.55\ \mu m < 2\pi k^{-1} < 0.82\ \mu m$. An in-depth study of this process and its relationship to biological function is presented in the previously mentioned reference.

V. Conclusions

As was discussed earlier, all the relevant statistical mechanical quantities for the description of fluid dynamics, as well as direct visualization of microscopic particle trajectories, can be gathered via digital video fluorescence microscopy experiments. However, the severe limitations of this technique, including long calculation times, excessive data storage requirements, and lack of readily available computing power for large sample systems, compels experimenters to find alternative methods for fluid characterization. Such techniques as dynamic light scattering and fluorescence correlation spectroscopy have opened many doors and provided much information to those that have used them, but still suffer from significant deficiencies in sensitivity and their ability to study delicate and/or complicated systems.

Nevertheless, Fourier imaging correlation spectroscopy (FICS), a new fluorescence technique independently developed by the Marcus Group, promises to overcome the deficiencies and limitations of the older techniques. Although the FICS experimental setup is similar to those employed by other methods used to study liquid state dynamics [Devoust, 1982; Hanson, 1998; Hattori, 1996], the focus of this past work has been to determine the bulk diffusion coefficient. Here, FICS has been used to quickly and directly measure the normalized intermediate scattering function, $F(k,\tau)/S(k)$, for a selectable $k = k_G$, something that neither DVFM nor other fluorescence techniques can boast. By disposing of the necessity of having a system possessing large, well-structure scattering centers, FICS experiments are able to perform measurements on complicated systems that DLS could never even begin to elucidate. With low excitation power requirements and high sensitivity, FICS is ideal for use with even the most delicate

systems, such as those encountered in biology. With all these advantages over the conventional methods of study, FICS proves to be a very useful, and certainly very important development in the field of fluid dynamics experimentation.

Acknowledgements

I would like to thank Prof. Andrew Marcus for his allowing me to work in his lab, and for everything I'd learned there during these past three years. I would also like to thank Michelle Knowles; a better partner, colleague, and friend would be hard to find. Thanks also go to the various other Marcus Group members throughout the years that have made working in the lab both an educational and enjoyable experience. Good luck to all.

References

B. J. Berne, R. Pecora, *Dynamic Light Scattering* (Krieger, Malabar, 1976).

P. N. Pusey, R. J. A. Tough, in *Dynamic Light Scattering: Applications of Photon Correlation Spectroscopy*, edited by R. Pecora (Plenum, New York, 1985).

J. Davoust, P. F. Devaux, L. Leger, *EMBO J.* **1**, 1233 (1982).

R. L. Hanson, X. R. Zhu, J. M. Harris, *Anal. Chem.* **70** 1281 (1998).

M. Hattori, H. Shimizu, H. Yokoyama, *Rev. Sci. Instrum.* **67**, 4064 (1996).

G. R. Fleming, *Chemical Applications of Ultrafast Spectroscopy* (Oxford University Press, New York, 1986).

P. Horowitz, W. Hill, *The Art of Electronics* (Cambridge University Press, New York, 1986).

D. Margineantu, R. A. Capaldi, A. H. Marcus, Biophys. J. (in press, 2000).

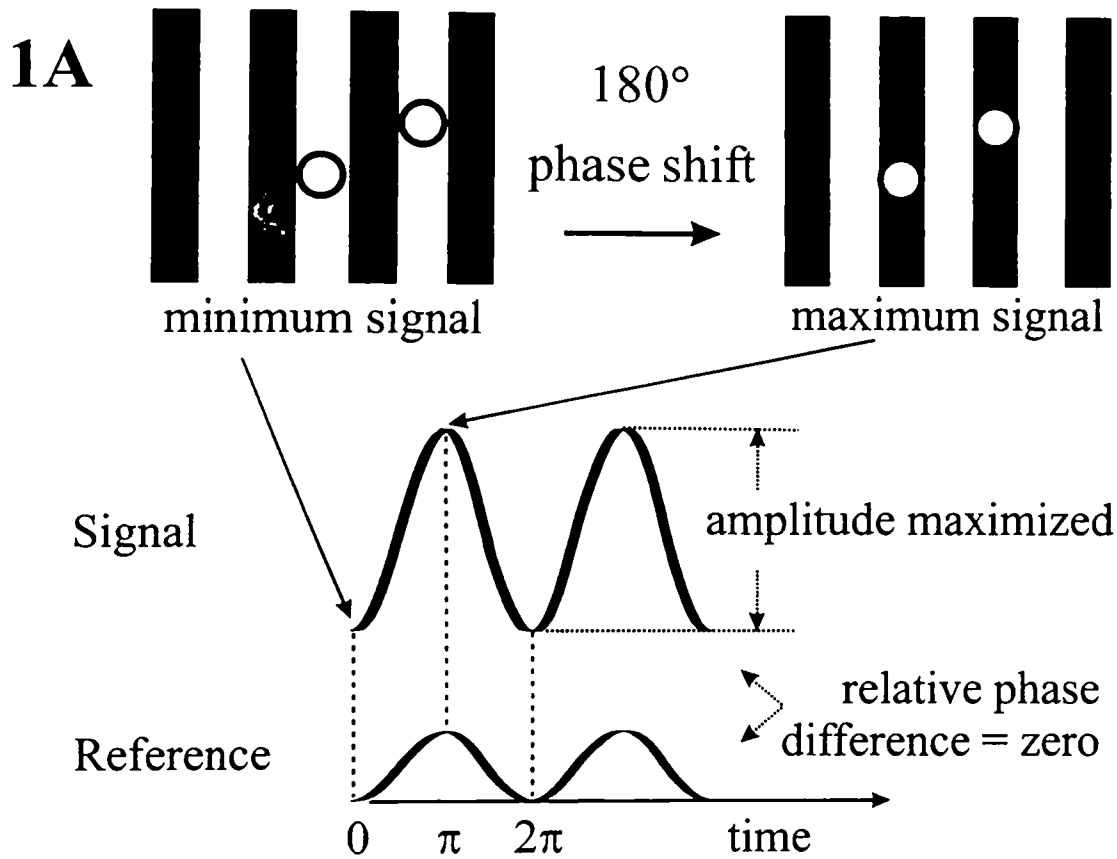
1A
180°
phase shift
minimum signal
maximum signal
Signal
amplitude maximized
relative phase
difference = zero
Reference
0
π
2π
time

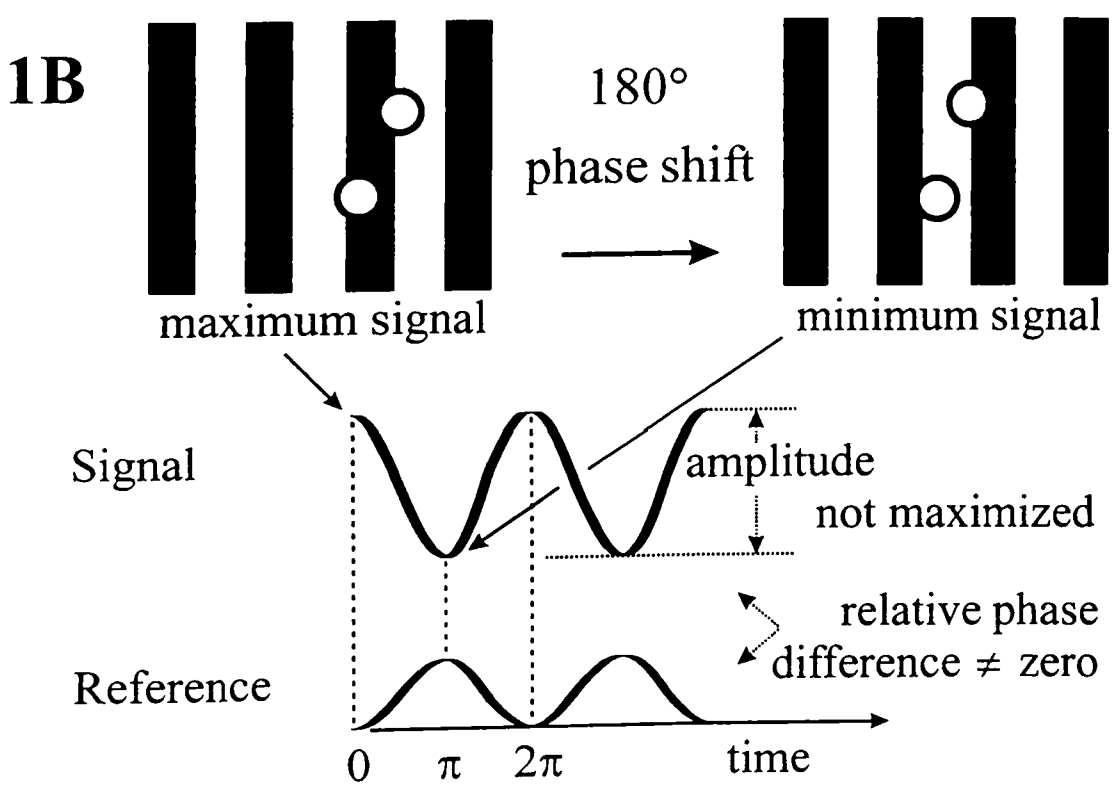
1B
180°
phase shift
maximum signal
minimum signal
Signal
amplitude
not maximized
relative phase
difference ≠ zero
Reference
0
π
2π
time

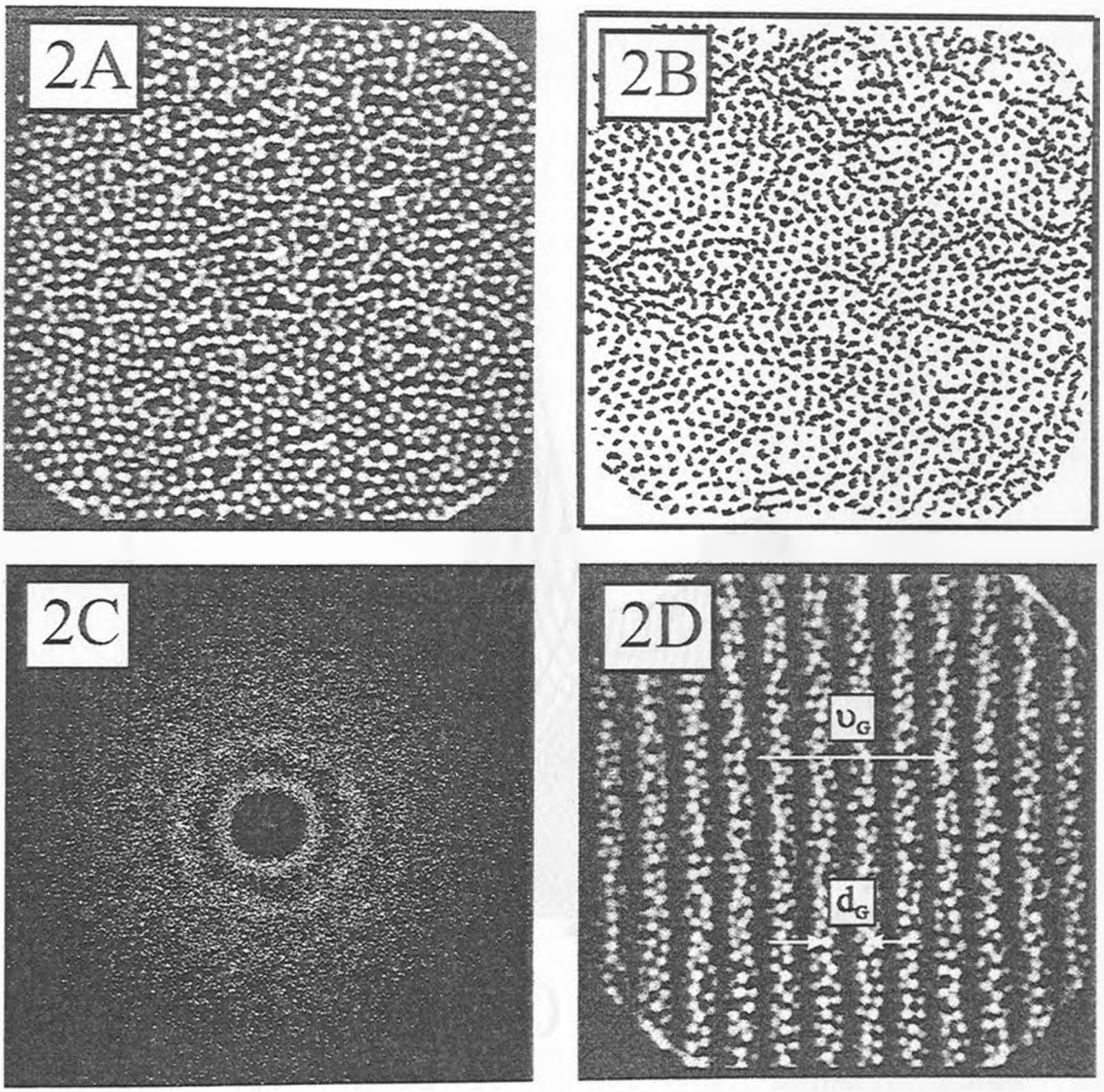
2A
2B
2C
2D
υ_G
d_G

3

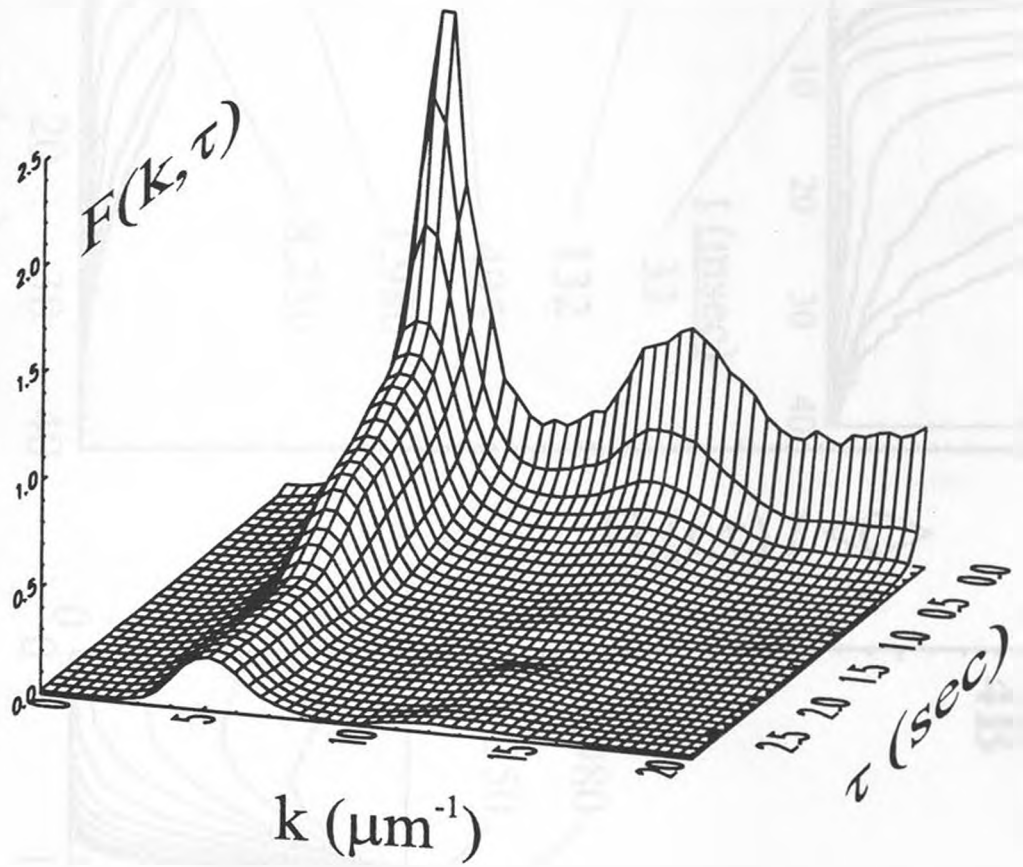

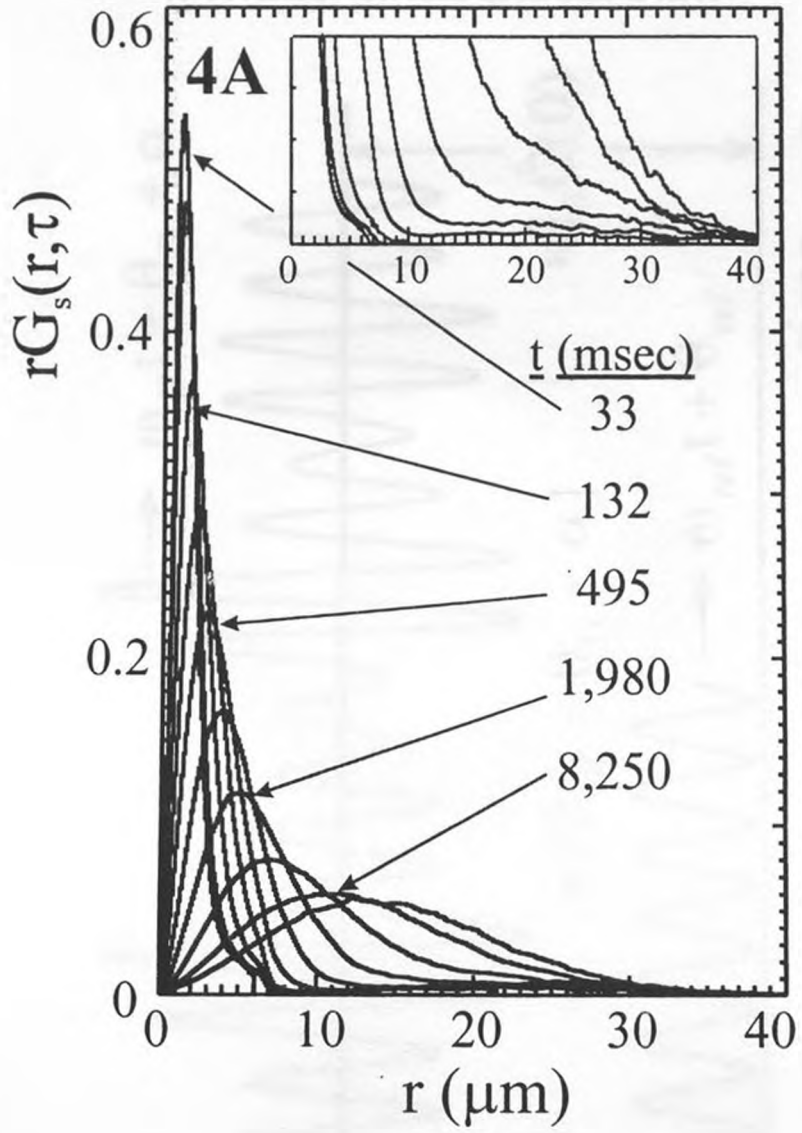
4A
0.6
0.4
0.2
0
0
10
20
30
40
rG_s(r,τ)
r (μm)
t (msec)
33
132
495
1,980
8,250

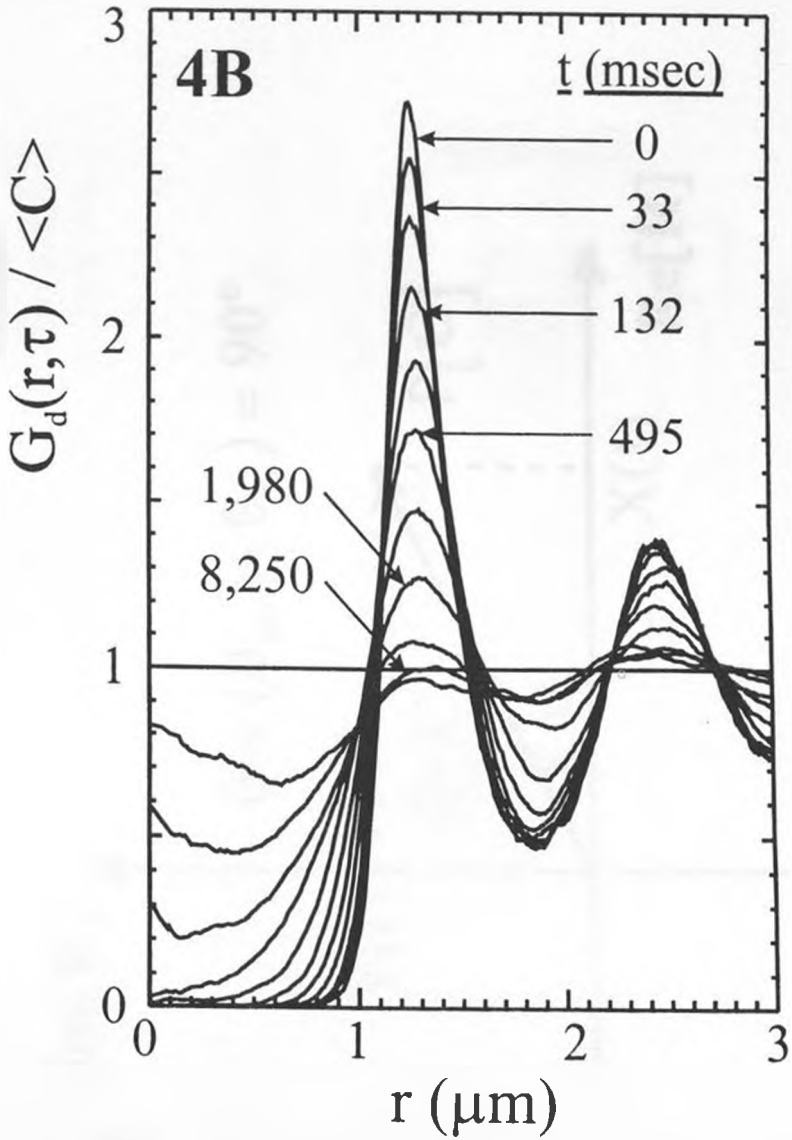
4B
t (msec)
0
33
132
495
1,980
8,250
$G_d(r,\tau) / \langle C \rangle$
r (μm)
0
1
2
3

5A

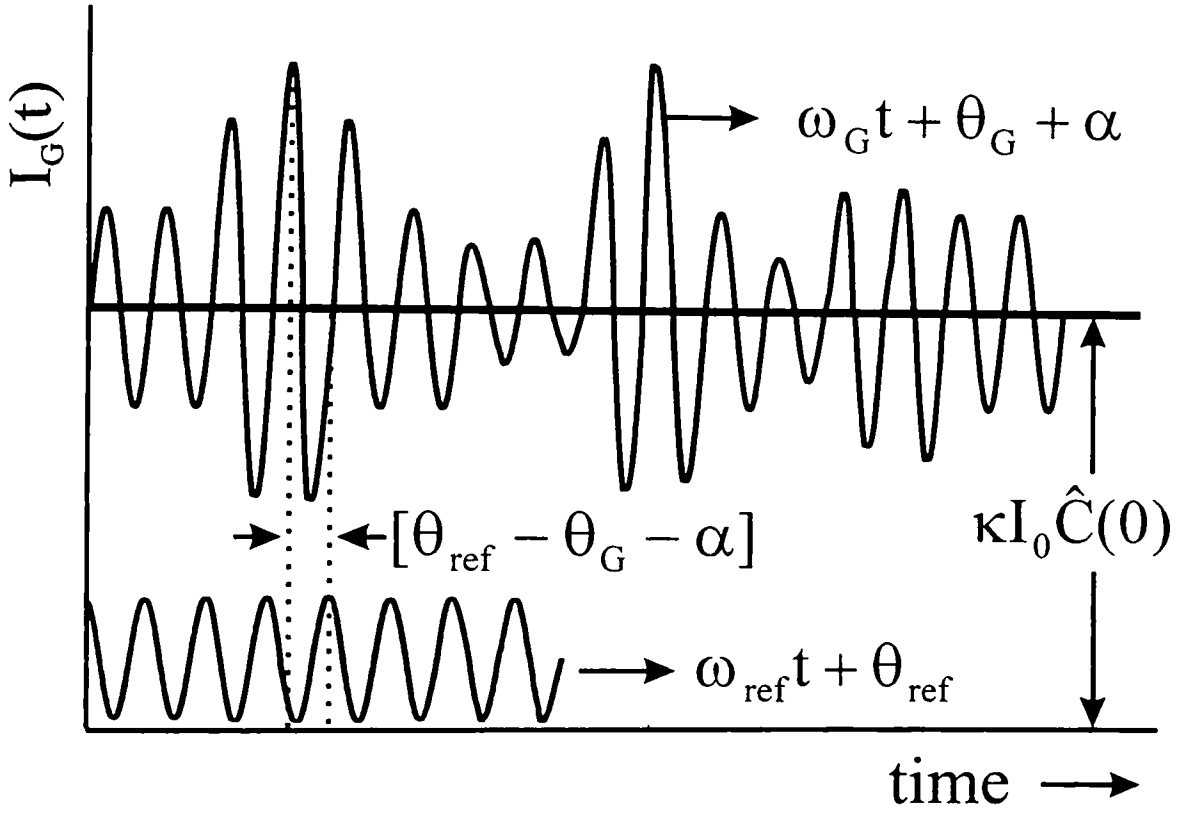
$I_G(t)$
$\omega_G t + \theta_G + \alpha$
$[\theta_{ref} - \theta_G - \alpha]$
$\kappa I_0 \hat{C}(0)$
$\omega_{ref} t + \theta_{ref}$
time

5B

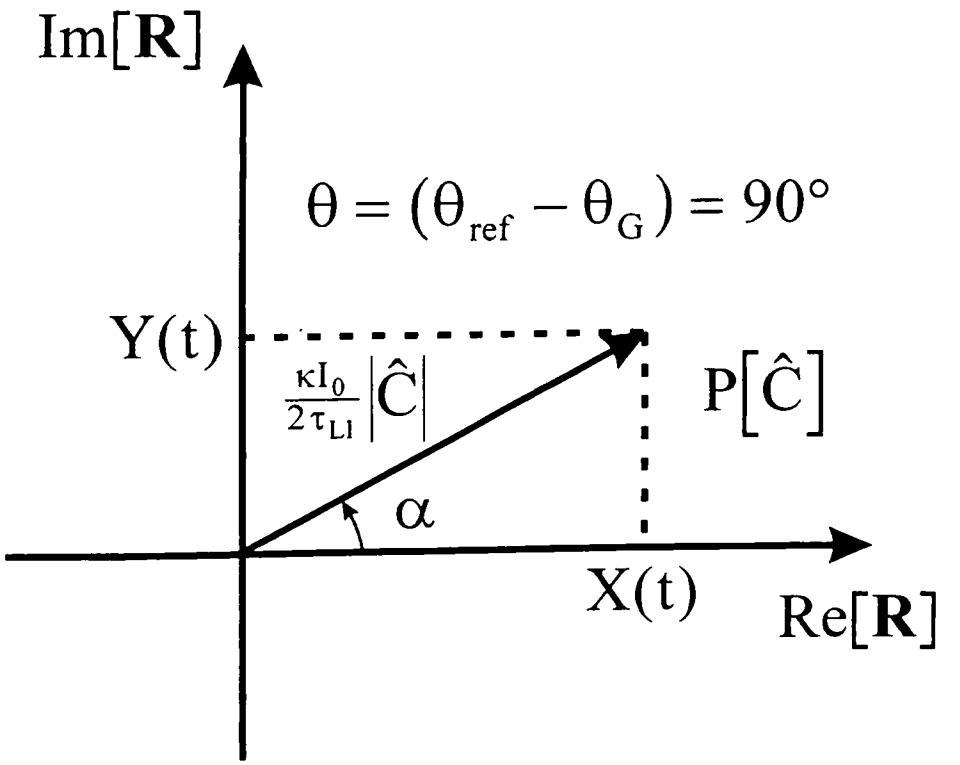
Im[**R**]
$\theta = (\theta_{ref} - \theta_G) = 90°$
Y(t)
$\frac{\kappa I_0}{2\tau_{LI}}|\hat{C}|$
$P[\hat{C}]$
α
X(t)
Re[**R**]

6A

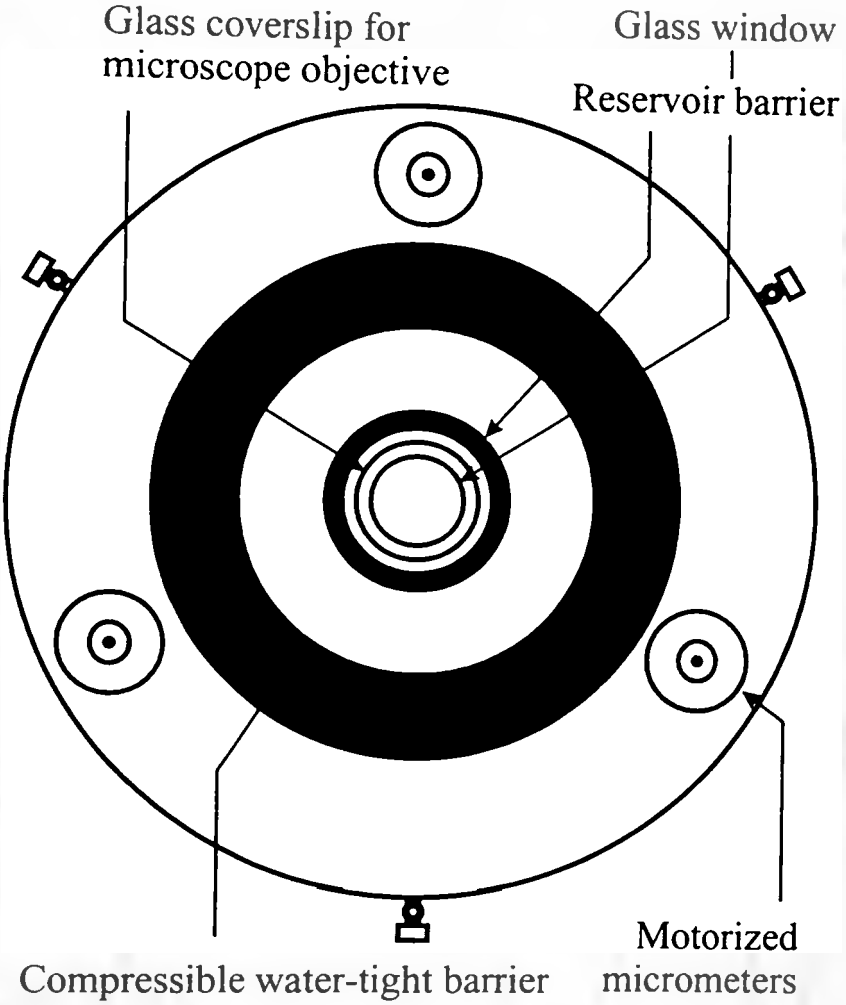
Glass coverslip for microscope objective
Glass window
Reservoir barrier
Compressible water-tight barrier
Motorized micrometers

6B

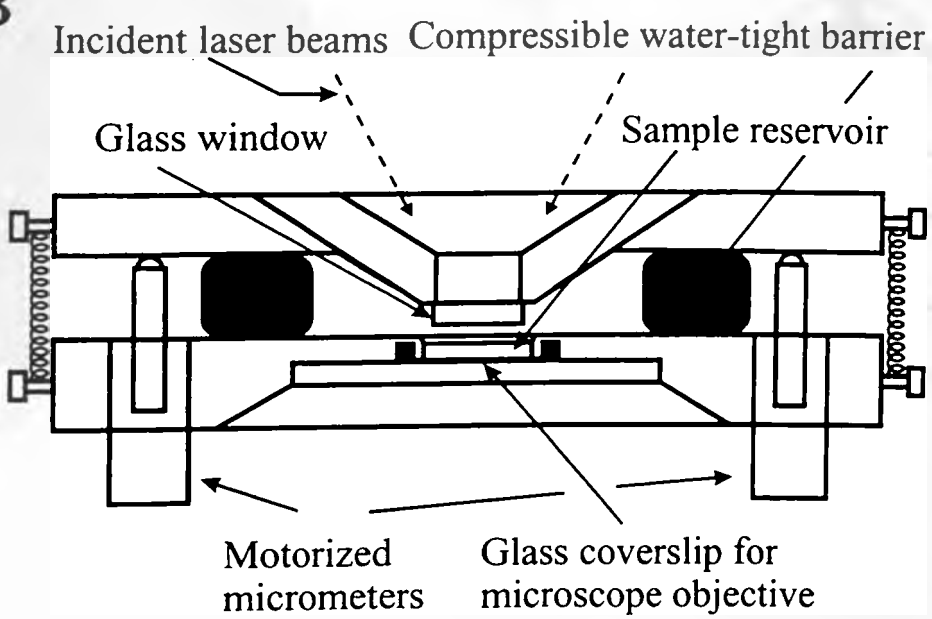
Incident laser beams
Compressible water-tight barrier
Glass window
Sample reservoir
Motorized micrometers
Glass coverslip for microscope objective

7

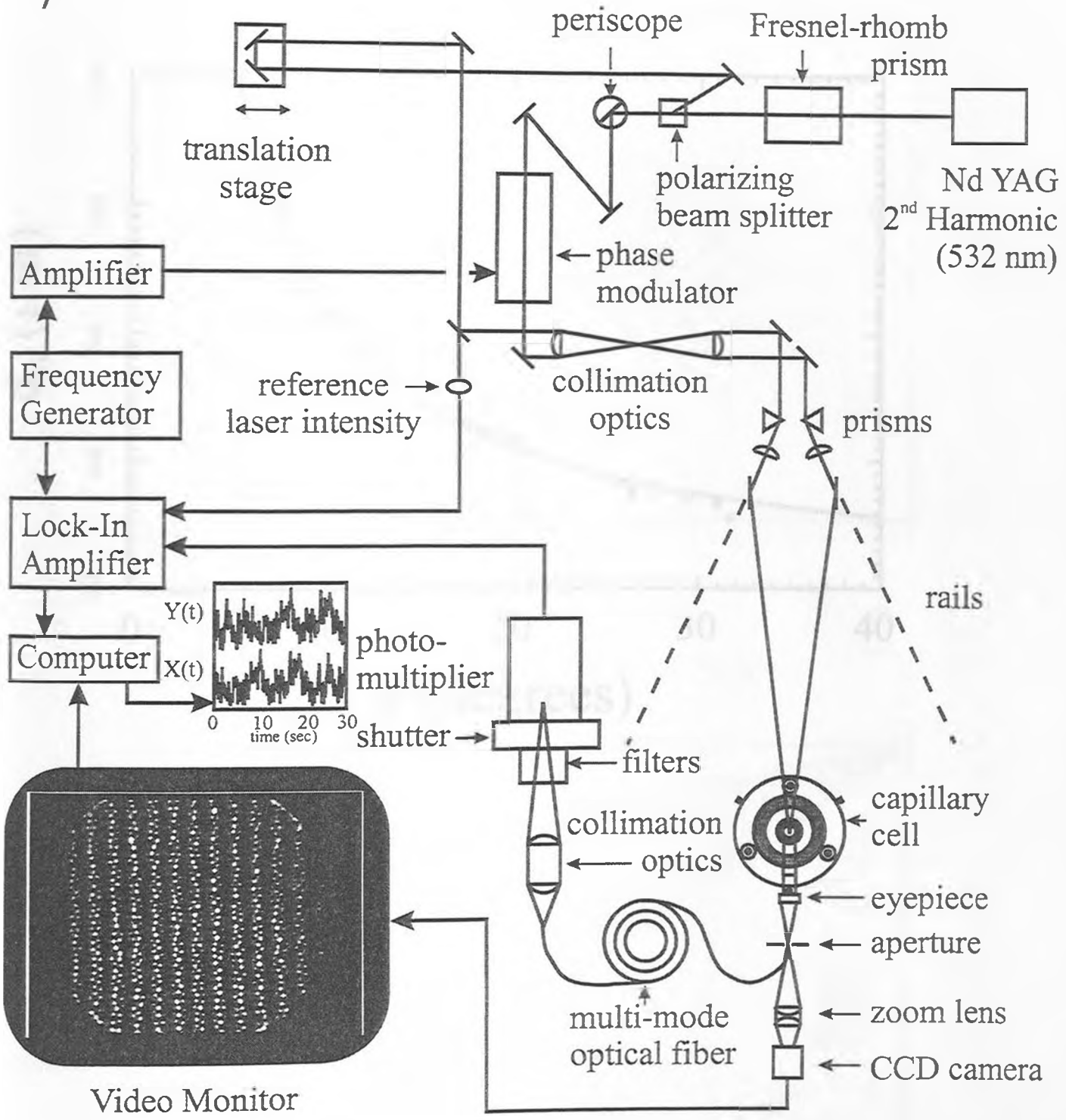
periscope
Fresnel-rhomb prism
translation stage
polarizing beam splitter
Nd YAG 2nd Harmonic (532 nm)
Amplifier
phase modulator
Frequency Generator
reference laser intensity
collimation optics
prisms
Lock-In Amplifier
rails
Y(t)
X(t)
Computer
photo-multiplier
0 10 20 30
time (sec)
shutter
filters
capillary cell
collimation optics
eyepiece
aperture
multi-mode optical fiber
zoom lens
CCD camera
Video Monitor

8

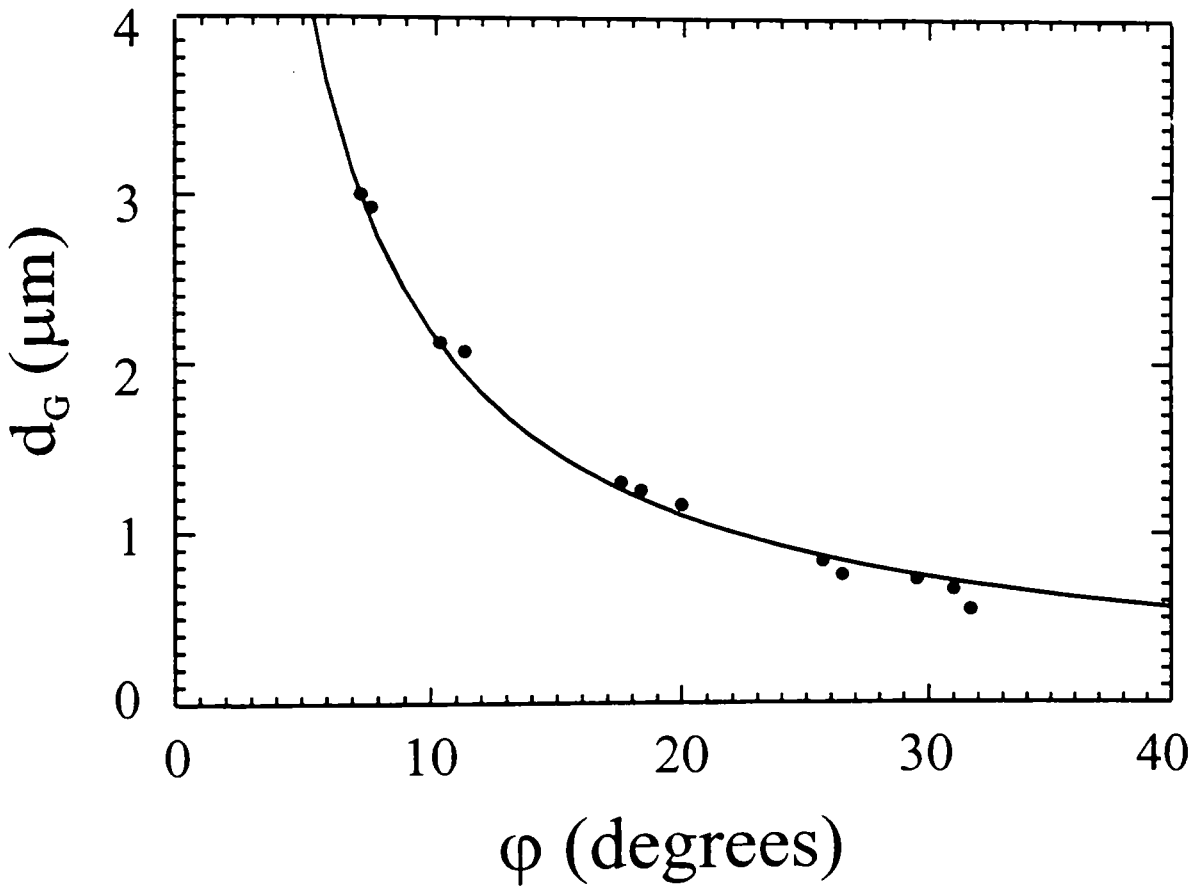

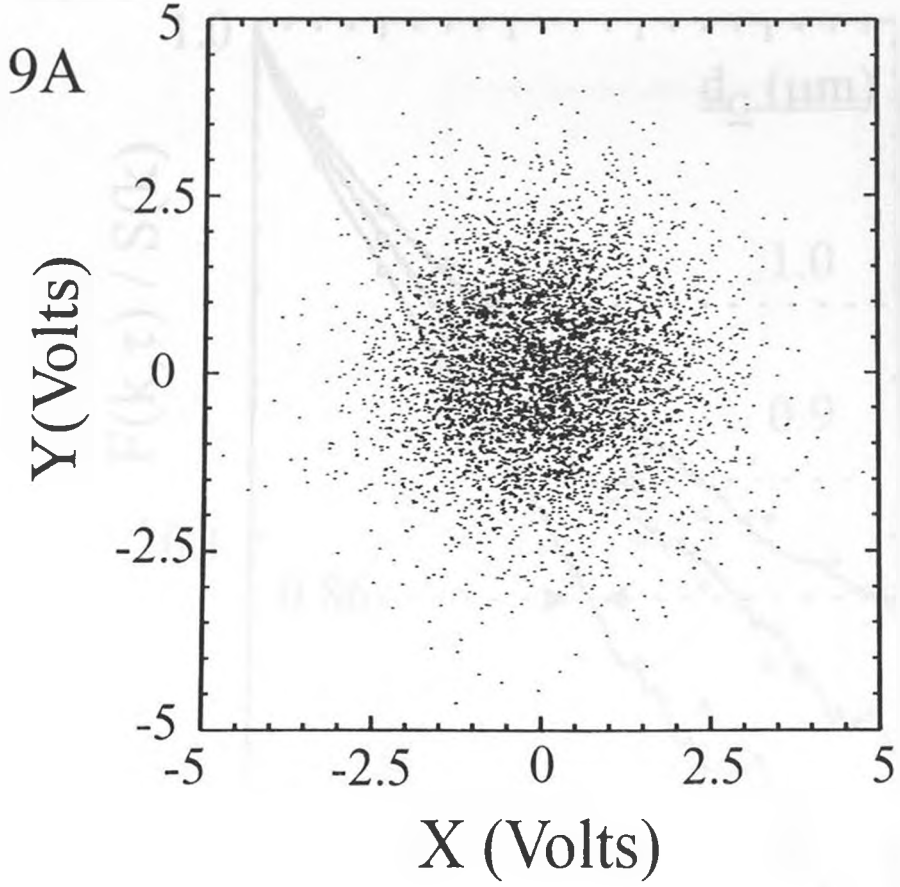
9A
5
2.5
0
-2.5
-5
Y(Volts)
-5
-2.5
0
2.5
5
X (Volts)

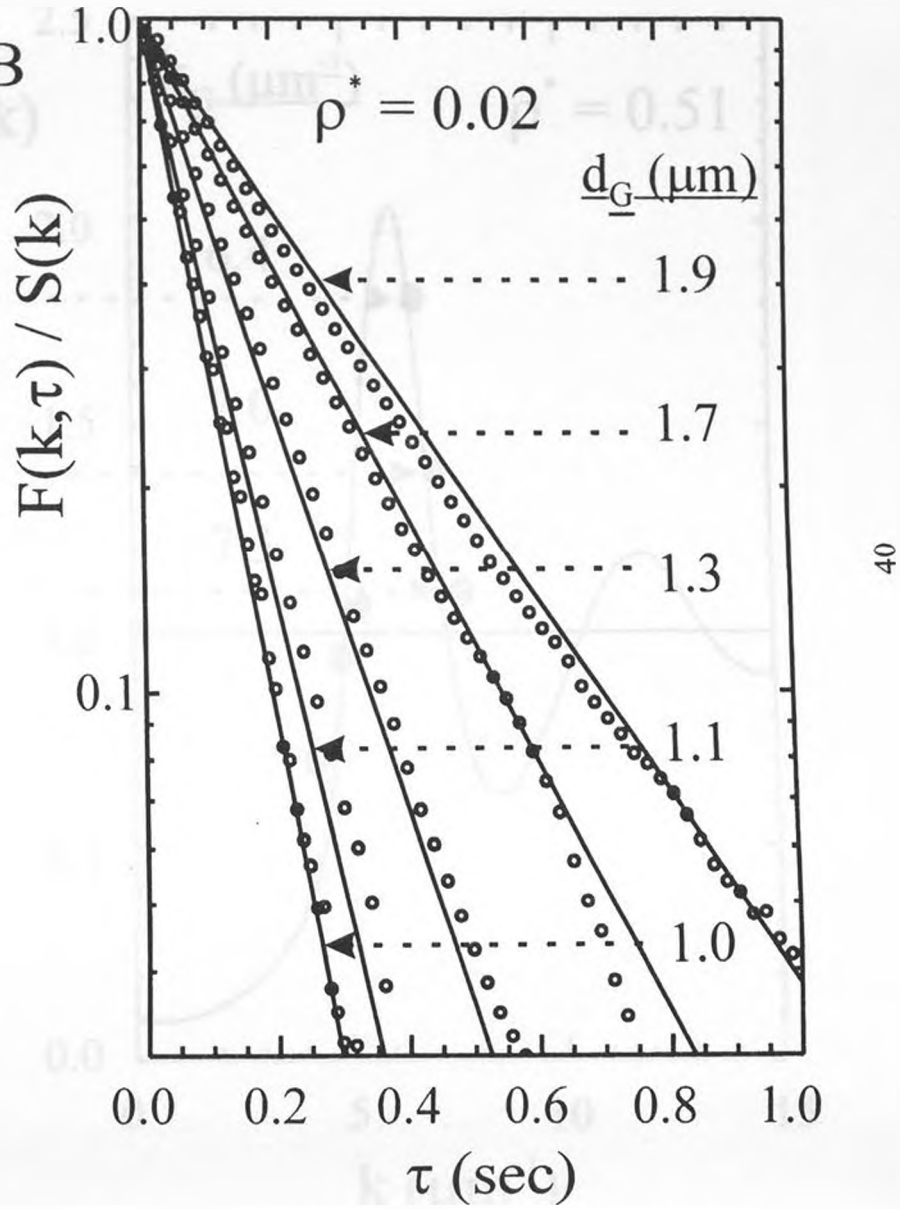
9B
1.0
0.1
$\rho^* = 0.02$
d_G (μm)
1.9
1.7
1.3
1.1
1.0
F(k,τ) / S(k)
0.0
0.2
0.4
0.6
0.8
1.0
τ (sec)

10A

10B

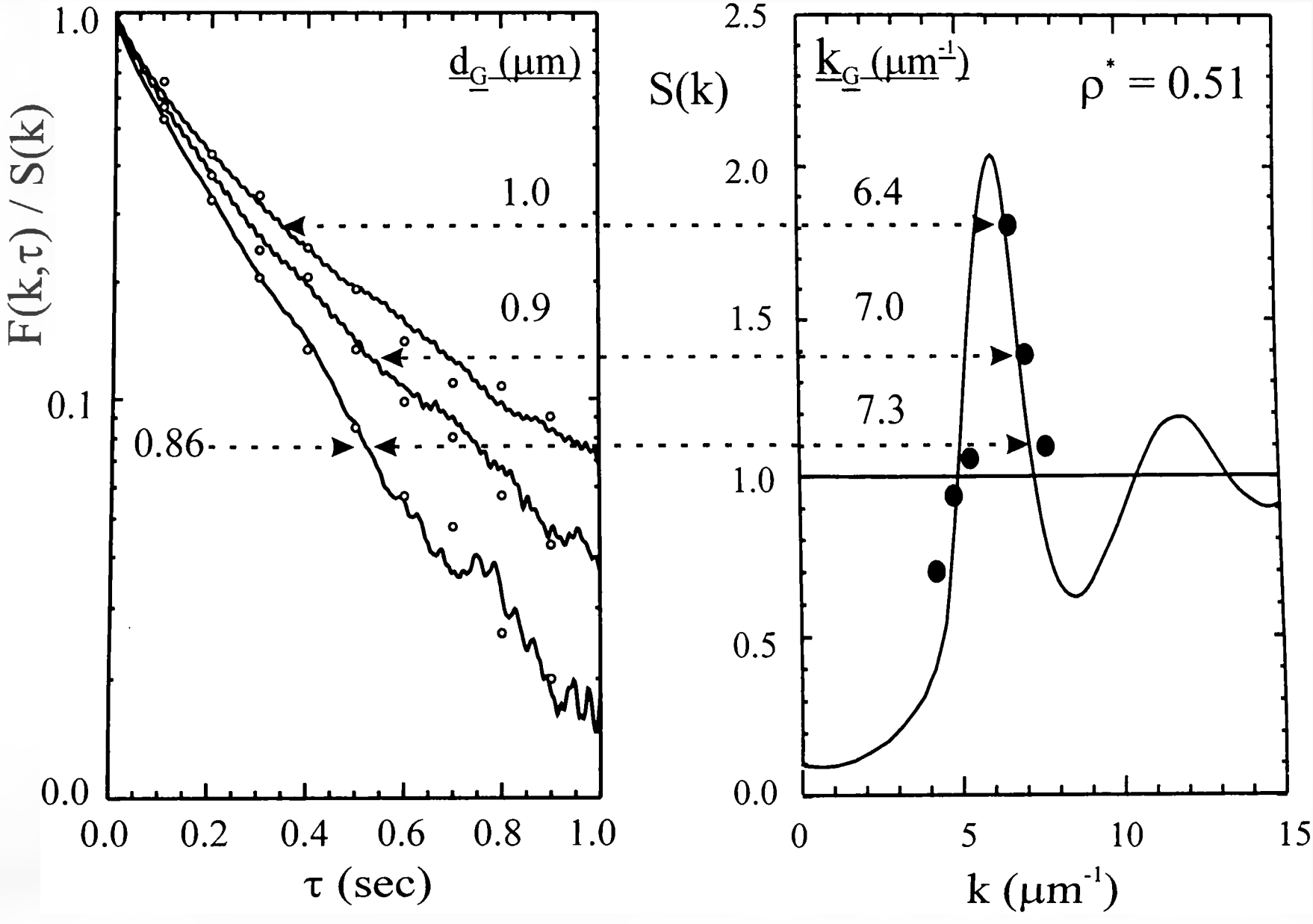
1.0
0.1
0.0
F(k,τ) / S(k)
d_G (μm)
1.0
0.9
0.86
0.0
0.2
0.4
0.6
0.8
1.0
τ (sec)
2.5
2.0
1.5
1.0
0.5
0.0
S(k)
k_G (μm^-1)
ρ* = 0.51
6.4
7.0
7.3
0
5
10
15
k (μm^-1)

11

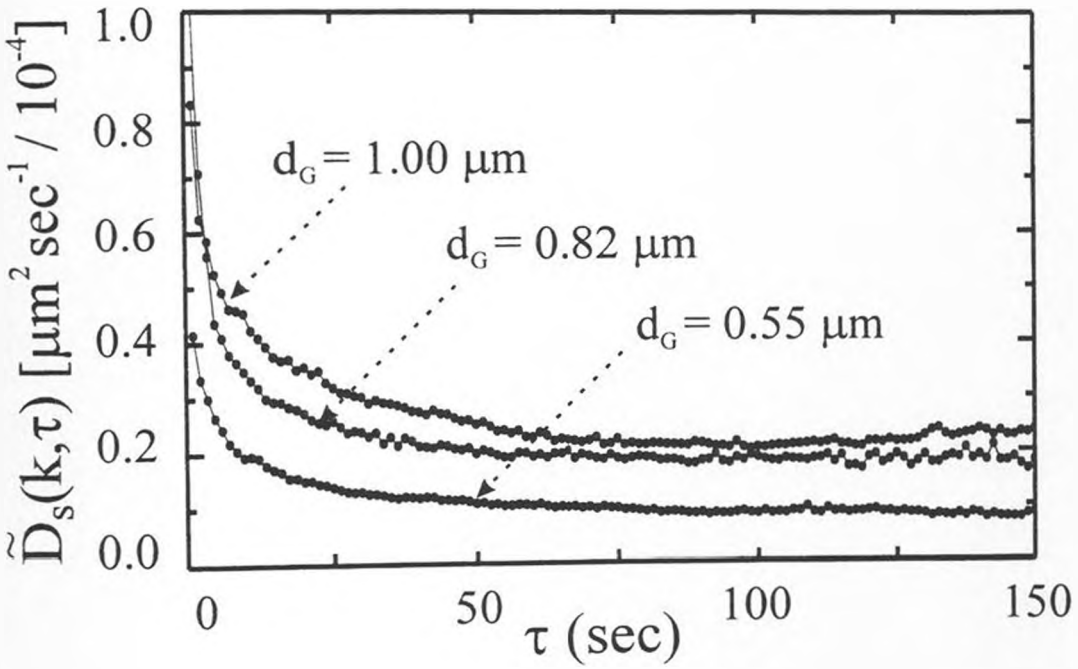
1.0
0.8
0.6
0.4
0.2
0.0
$\tilde{D}_s(k,\tau)$ [$\mu m^2 sec^{-1} / 10^{-4}$]
d_G = 1.00 μm
d_G = 0.82 μm
d_G = 0.55 μm
0
50
100
150
τ (sec)